www.MaterialsViews.com

A S-Layer Protein of *Bacillus anthracis* as a Building Block for Functional Protein Arrays by In Vitro Self-Assembly

Xu-Ying Wang, Dian-Bing Wang, Zhi-Ping Zhang, Li-Jun Bi, Ji-Bin Zhang, Wei Ding, and Xian-En Zhang**

***S**-layer proteins create a cell-surface layer architecture in both bacteria and archaea. Because S-layer proteins self-assemble into a native-like S-layer crystalline structure in vitro, they are attractive building blocks in nanotechnology. Here, the potential use of the S-layer protein EA1 from Bacillus anthracis in constructing a functional nanostructure is investigated, and apply this nanostructure in a proof-of-principle study for serological diagnosis of anthrax. EA1 is genetically fused with methyl parathion hydrolase (MPH), to degrade methyl parathion and provide a label for signal amplification. EA1 not only serves as a nanocarrier, but also as a specific antigen to capture anthrax-specific antibodies. As results, purified EA1–MPH forms a single layer of crystalline nanostructure through self-assembly. Our chimeric nanocatalyst greatly improves enzymatic stability of MPH. When applied to the detection of anthrax-specific antibodies in serum samples, the detection of our EA1–MPH nanostructure is nearly 300 times more sensitive than that of the unassembled complex. Together, it is shown that it is possible to build a functional and highly sensitive nanosensor based on S-layer protein. In conclusion, our present study should serve as a model for the development of other multifunctional nanomaterials using S-layer proteins.*

1. Introduction

In biological systems, a large number of nanostructures, including fibers, tubes, rings, cages, and viruses have been identified. These nanoarchitectures are formed through spontaneous self-assembly of biomolecules such as nucleic acids, lipids, peptides, and proteins. Because these biomolecules self-assemble into uniform and ultrasmall units, they have been used in a wide range of applications in nanotechnology, where they are of great interest for developing nanoreactors, matrix scaffolds, nanocarriers, and other functional nanomaterials.[1]

X.-Y. Wang, Prof. D.-B. Wang, Prof. L.-J. Bi, Prof. X.-E. Zhang
National Laboratory of Biomacromolecules
Institute of Biophysics
Chinese Academy of Sciences
Beijing 100101, China
E-mail: wangdb@moon.ibp.ac.cn; zhangxe@ibp.ac.cn

X.-Y. Wang, Prof. J.-B. Zhang
State Key Laboratory of Agromicrobiology
College of Life Science and Technology
Huazhong Agricultural University
Wuhan 430070, China

Prof. Z.-P. Zhang
State Key Laboratory of Virology
Wuhan Institute of Virology
Chinese Academy of Sciences
Wuhan 430071, China

Dr. W. Ding
Center for Biological Imaging
Institute of Biophysics
Chinese Academy of Sciences
Beijing 100101, China

DOI: 10.1002/smll.201501413

The cell-surface layer (S-layer) is a self-assembled protein architecture that forms the outermost surface of some bacteria and archaea. The S-layer is composed of a single protein or glycoprotein, with a molecular mass ranging from 40 to 230 kD, depending on its bacterial origin.[2] In different species, the S-layer consists of regular 2D crystalline arrays, exhibiting either an oblique (p1, p2), square (p4), or hexagonal (p3, p6) lattice symmetry.[3] Previous studies have shown that S-layer proteins can self-assemble into a native-like S-layer crystalline structure on solid surfaces and interfaces.[4] This self-assembling property of S-layer proteins might serve as prerequisite for their application in synthetic biology, biomimetics, and nanotechnology.[5] It was reported previously that S-layers can improve the performance of certain electrodes, DNA microarrays, microchips, and cellular micropatterning.[6] Because of the high densities of their nanosized pores and the presence of chemical groups on their surface, S-layers were also reported to be useful for ultrafiltration as well as for the synthesis of inorganic nanocrystals.[7] Besides, specific proteins such as streptavidin, enzymes, and antibodies can be linked with S-layer proteins to construct versatile nanostructures with multiple functions.[8] During the last three decades, the knowledge of the defined crystal structures and the assembling process of S-layers has grown rapidly, it is now feasible to design novel S-layer-based lattices using computational design.[9] These reported studies have shown great interests on S-layer proteins for their self-assembly ability, as well as related physicochemical properties. However, many intrinsic biological characteristics of S-layer proteins were neglected, which will to some degree restrict applications of S-layer proteins in nanotechnology.

The S-layer protein of *Bacillus anthracis* EA1 is the most active avirulent antigen in both serological and cellular reactions, with 861 amino acids and a signal peptide of 29 amino acids at the N-terminal.[10] This protein can induce anti-anthrax immune responses. In the process of infection, specific antibodies are produced in the host, conferring protection against *B. anthracis*.[11] Thus, it was previously suggested that it can be used to test for specific humoral and cell-mediated anti-anthrax immune responses.[12]

The aim of this study is to develop an S-layer–enzyme conjugate for high sensitive detection of anthrax antibodies. The enzyme we used is methyl parathion hydrolase (MPH), which was isolated from *Pseudomonas* sp. WBC-3,[13] and shows good catalytic activity.[14] In particular, it is a monomer in solution and its 3D structure is known. Because of these features, MPH is recommended as a new analytical enzyme.[15]

In this study, we demonstrated successfully that EA1 self-assembled into an S-layer lattice structure in vitro, and constructed an EA1-based 2D nanostructure containing MPH, which was arranged in an orderly fashion, allowing for the degradation of methyl parathion and the detection of anthrax antibodies. This nanostructure obviously enhances stability of enzymatic activity. This nanocatalyst possesses high detection sensitivity, which is comparable to existing methods,[16] and can be used as a model for other immunoassays. Here, we established a proof-of-principle that S-layer-based nanomaterials can be endowed with new functions by combining the self-assembly ability of S-layer proteins with their intrinsic biological characteristics.

2. Results and Discussions

2.1. Construction of $EA1_{30}$, MPH, and $EA1_{30}$–MPH

EA1 with a signal peptide of 29 amino acids truncation at N-terminal ($EA1_{30}$) and its fusion protein with MPH ($EA1_{30}$–MPH) were investigated for their expressions in *Escherichia coli* M15 by sodium dodecyl sulfate–polyacrylamide gel electrophoresis (SDS–PAGE) analysis. As shown in Figure S (Supporting Information), $EA1_{30}$–MPH, $EA1_{30}$, and MPH were overexpressed as soluble forms in *E. coli* M15, and these proteins were obtained by His-Tag affinity purification (Figure S, Supporting Information). The molecular mass of purified proteins were 124 kDa, 90 kDa, and 34 kDa for $EA1_{30}$–MPH, $EA1_{30,}$ and MPH, respectively, as shown by gel electrophoresis (Figure S, Supporting Information).

2.2. Recrystallization of $EA1_{30}$ and $EA1_{30}$–MPH In Vitro

To test whether the truncated form $EA1_{30}$ possesses self-assembly properties in aqueous solution, we employed TEM analysis. The purified proteins were dialyzed in assembly buffer at either 25 °C or 4 °C for 5 or 12 h. Subsequently, the dialyzed proteins were placed on a TEM grid according to standard EM procedure (see Experimental Section). We found that these truncated proteins recrystallized under these conditions. When incubated at 4 °C for 12 h, $EA1_{30}$ proteins formed the most regular 2D crystalline arrays (data not shown). $EA1_{30}$ proteins self-assembled into regular monomolecular layer (**Figure 1**a,b,e), with the unit cells displaying the following parameters: a = 73 Å, b = 83 Å, γ = 112°. As shown in Figure 1, the sheet displayed a nanostructure of p1 symmetry, which was identical to the previously reported structure of a natural S-layer in *B. anthracis*.[17] To identify which region within EA1 is essential for its self-assembly, we truncated either 229 aa or 429 aa from both N-terminus and C-terminus, which were named as $EA1_{N\text{-}230}$, $EA1_{N\text{-}430,}$ and $EA1_{C\text{-}230}$, $EA1_{C\text{-}430}$. We found that only $EA1_{N\text{-}230}$ maintained the ability of self-assembly into monolayers in solutions. However, this sheet had no clear and regular lattice structure (data not shown). These results indicated that deletion of these amino acids disrupted the self-assembly property of EA1. Therefore, only the truncated $EA1_{30}$ was chosen as a carrier for subsequent experiments.

Next, we combined MPH with $EA1_{30}$ and tested if the self-assembly process still occurred. As shown in Figure 1f,g,j, $EA1_{30}$–MPH also formed a highly order monolayer, which showed the same p1 symmetry as $EA1_{30}$ alone with slightly altered unit cell parameters (a = 62 Å, b = 71 Å, γ = 135°).

2.3. MPH Activity and Stability of Recombinant Protein $EA1_{30}$–MPH

The activity of recombinant MPH either alone or in complex with $EA1_{30}$ ($EA1_{30}$–MPH) was determined in both assembly buffer and control buffer. The control buffer was used to keep proteins in monomeric state and acted as an ideal buffer for enzymatic reactions. In the assembly buffer, $EA1_{30}$

www.MaterialsViews.com

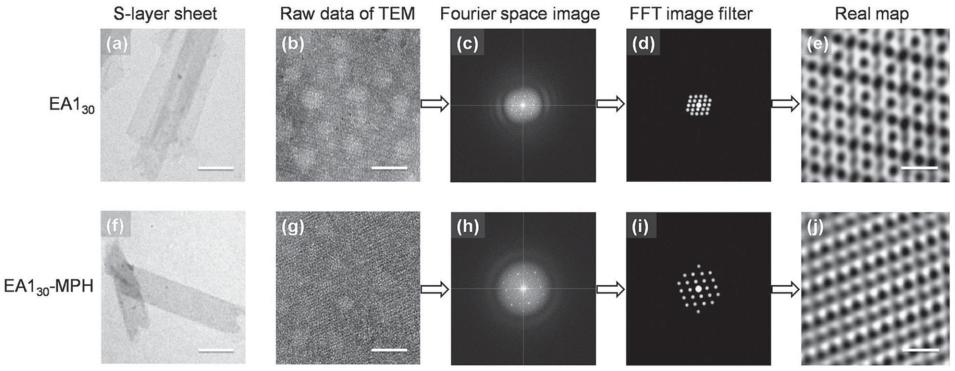

Figure 1. Transmission electron microscopy (TEM) analysis of self-assembled S-layers of EA1$_{30}$ and EA1$_{30}$–MPH. a,f), respective S-layer sheets of EA1$_{30}$ and EA1$_{30}$–MPH; b,g), enlarged S-layer sheets of EA1$_{30}$ and EA1$_{30}$–MPH; c,h), fast Fourier transforms of b,g); d,i), spot masks for maps c,h) obtained by FFT (fast Fourier transform) image filter; e,j), real maps from invert FFT of d) and i), which reveal the regular structure of the S-layer sheet of EA1$_{30}$ and the altered regular structure of the S-layer sheet of EA1$_{30}$–MPH, respectively. Scale bars: a,f) 500 nm, b,g) 50 nm, and e,j) 10 nm.

and EA1$_{30}$–MPH proteins formed a monomolecular nanostructure with regular crystal lattices. As shown in **Figure 2**, EA1$_{30}$–MPH exhibited similar MPH activity as monomeric MPH, both of which were diluted in the control buffer. Together, these results showed that fusion with EA1 had no significant impact on MPH activity of MPH.

Next, we compared the activities of EA1$_{30}$–MPH and MPH in the assembly and control buffers using a colorimetric assay. Our results showed that in the assembly buffer, both EA1$_{30}$–MPH and MPH displayed slightly decreased enzyme activity relative to control buffer. Presumably, this was due to the different concentrations of Ca^{2+} and the difference in pH value between these two buffers.

To investigate the effect of storage temperature on the enzymatic activity of EA1$_{30}$–MPH and MPH, the proteins were stored at 4 °C and at 37 °C, respectively, in the absence of preservatives. The enzymatic activity of MPH in control buffer at time-point zero was defined as 100%. At 4 °C, the assembled EA1$_{30}$–MPH maintained 70% enzymatic activity over the course of 45 d, while the activities of monomeric EA1$_{30}$–MPH and MPH were significantly decreased over the same time span (below 20%, see **Figure 3**a). At 37 °C, the assembled EA1$_{30}$–MPH form displayed a slow reduction in activity, reaching approximately 25% of starting activity.

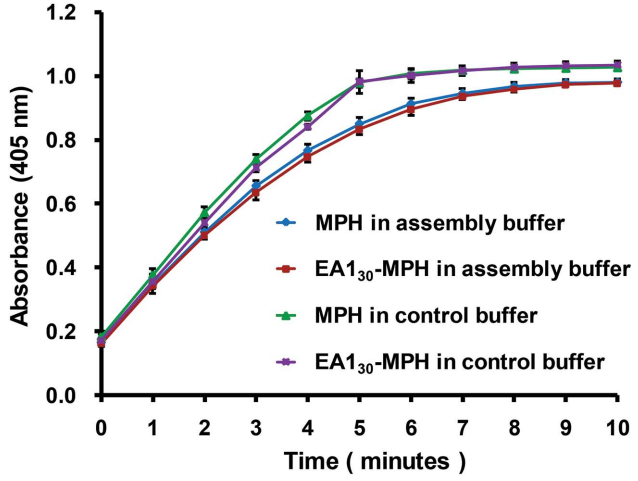

Figure 2. The methyl parathion hydrolase activity of EA1$_{30}$–MPH and MPH. Assembly buffer: 10×10^{-3} M $CaCl_2$, 0.5×10^{-3} M tris–HCl, pH 9.0; control buffer: 0.5×10^{-3} M tris–HCl, pH 7.0.

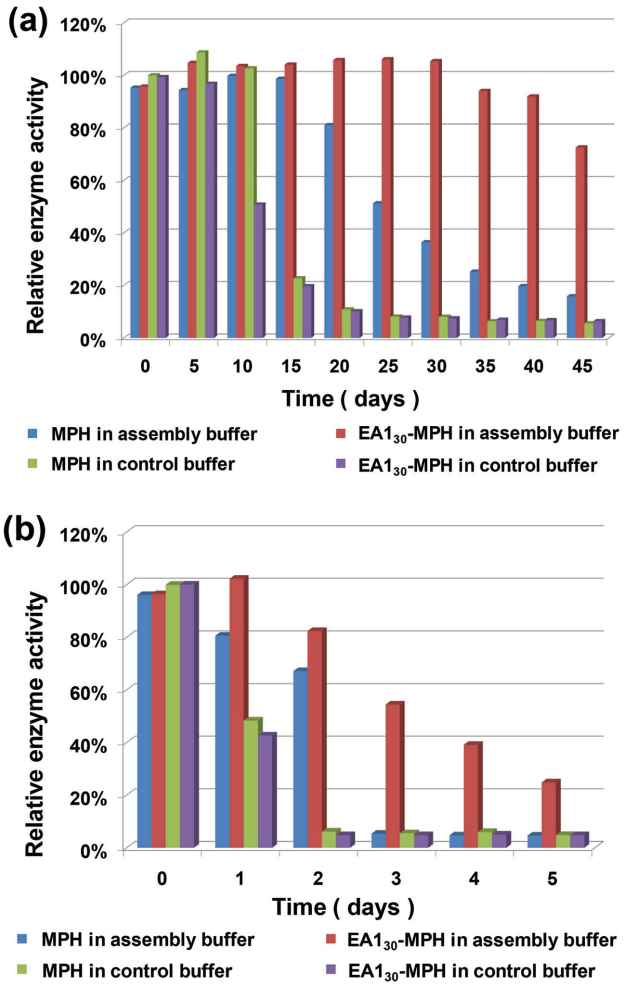

Figure 3. Enzyme stability analysis. The enzyme stability of EA1$_{30}$–MPH and MPH at a) 4 °C and b) 37 °C. Assembly buffer: 10×10^{-3} M $CaCl_2$, 0.5×10^{-3} M tris–HCl, pH 9.0; control buffer: 0.5×10^{-3} M tris–HCl, pH 7.0. The enzyme activity of MPH in control buffer at 0 day was defined as 100%.

small NANO MICRO

In contrast, the activities of monomeric $EA1_{30}$–MPH and MPH were reduced to below 10% after only 2 d of storage (green and purple bars in Figure 3). Importantly, $EA1_{30}$ greatly increased the long-term stability of MPH upon assembly (red bar in Figure 3), relative to MPH alone in assembly buffer (blue bar in Figure 3), presumably because the rate of degradation of MPH molecules was greatly reduced upon incorporation into the EA1 layer. In comparison, the monomeric proteins lost 90% of their enzymatic activity after 3 d of storage at 37 °C.

In summary, in addition to the improved self-assembly, the enzyme stability of MPH was greatly increased by fusion to EA1. These results suggest that in theory, any enzymatic moiety can be incorporated into such a nanostructure in order to improve its overall activity as well as long-term stability.

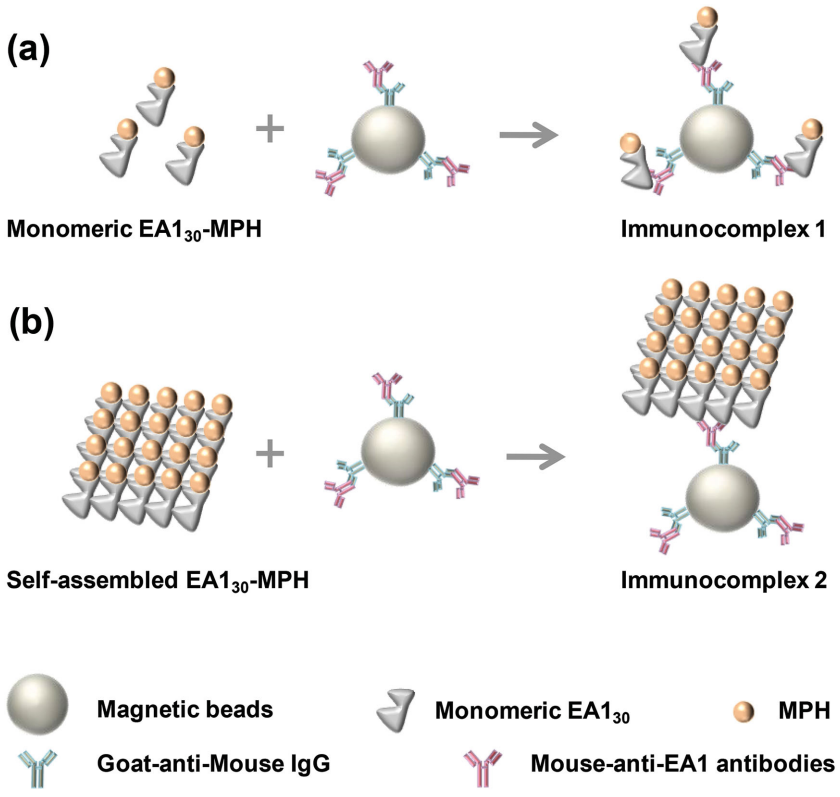

Figure 4. Schematic illustration of the detection of anthrax antibodies with monomeric a) $EA1_{30}$–MPH and b) self-assembled $EA1_{30}$–MPH.

2.4. $EA1_{30}$–MPH-Based Nanostructure for the Detection of Anthrax

Since we showed that MPH activity is retained upon assembly in EA1 layer, we next wanted to test whether this nanostructure could be used to detect clinically relevant biomaterial at improved sensitivity. **Figure 4** shows the detection of anthrax antibodies with $EA1_{30}$–MPH. In this protocol, goat anti-mouse antibodies were immobilized on magnetic particles to capture murine antibodies. Among these antibodies, the anti-EA1 antibodies were recognized by both monomeric $EA1_{30}$–MPH and self-assembled $EA1_{30}$–MPH. After washing and mixing with methyl parathion, which is the substrate of MPH, the anti-EA1 antibodies were detected by determining the absorption at 405 nm or by color changes. In this work, mouse samples were used for proof-of-principle testing. However, the self-assembled $EA1_{30}$–MPH is also applicable for the detection of human and the other *B. anthracis* infected animals such as sheep, cattle, as long as the magnetic particles are conjugated with the appropriate secondary antibodies.

As shown in **Figure 5**a, monomeric $EA1_{30}$–MPH detected purified antibodies at concentrations as low as 25 ng mL^{-1} within 1 h, while the self-assembled $EA1_{30}$–MPH displayed a detection limit of about 0.1 ng mL^{-1}. These data indicated that $EA1_{30}$–MPH present in a crystalline structure improved the detection sensitivity by more than 250 times. As shown in Figure 5b, these changes were observed even without the use of any additional methods, other than by visual observation. Crucially, our $EA1_{30}$–MPH S-layer displayed both superior sensitivity over monomeric $EA1_{30}$–MPH, as well as high signal specificity, indicating that the S-layer also prevented interference of other molecules present in complex biological specimen such as blood serum. As showed in Figure 5c,d, the detection limit of antibodies by the self-assembled $EA1_{30}$–MPH in the serum sample was still 0.1 ng mL^{-1}.

Bindings of $EA1_{30}$–MPH sheet to antibodies conjugated magnetic particles were observed under transmission electron microscopy. As shown in **Figure 6**, when $EA1_{30}$–MPH was assembled into a nanomembrane, a large piece of this sheet was captured by the conjugates of magnetic particles and antibodies. Thus, the resulting ratio of signal (MPH) to conjugates was drastically increased in the case of nanomembrane when compared with the ratio achieved by monomeric $EA1_{30}$–MPH forms. The ensuing amplification greatly improved the sensitivity of this assay. Also, the formation of the nanomembrane creates a microenvironment, which increases the probability of interaction between anthrax antibody and $EA1_{30}$–MPH, thus allowing for higher rates of signal generation. Together, these results convincingly show that the $EA1_{30}$–MPH nanolayer displays a far higher detection sensitivity than monomeric $EA1_{30}$–MPH. In summary, our novel nanostructure based on $EA1_{30}$–MPH units should greatly facilitate the diagnosis of anthrax on the basis of anthrax antibodies in serum samples, particularly because of its vastly superior sensitivity and specificity of detection. Importantly, our assay allows for fast and simple visual assessment, without the need for specialized equipment or refrigeration, making it ideally suited for use under field conditions.

In the future, a combination of our nanomaterial presented here with portable biosensors should allow for the development of a vast array of applications for the detection

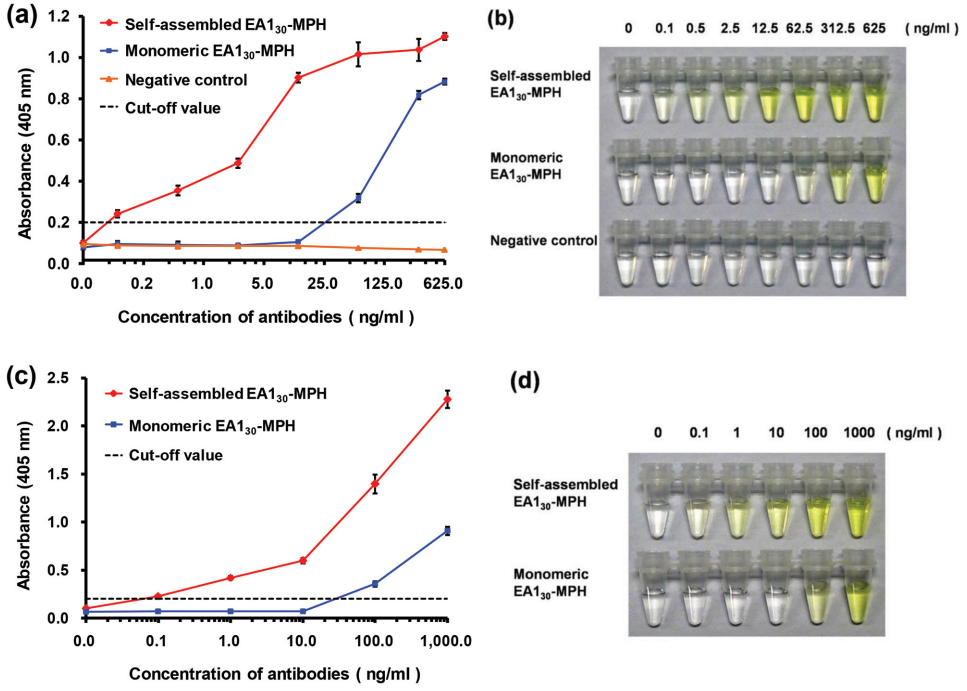

Figure 5. Detection of anti-EA1 antibodies using monomeric EA1$_{30}$–MPH and self-assembled EA1$_{30}$–MPH. a) The purified antibodies were detected using a BioTek enzyme standard instrument (Synergy H1). b) Representative samples are shown. c) Reactions in serum samples were measured using a spectrometer. d) Representative samples are shown. Each test was repeated at least three times. M13 phage antibodies were used as the negative control. The dashed line presents the cut-off value of 0.2 and a signal to noise ratio (S/N) of ≥2.

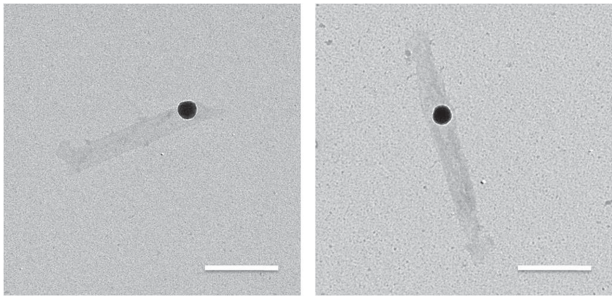

Figure 6. TEM images of the immunocomplexes of self-assembled EA1$_{30}$–MPH and antibodies/anti-anthrax antibodies modified magnetic particles. Scale bars: 1 μm.

of biological agents and diagnosis of infectious disease both in the clinic and the field.

3. Conclusion

Our work presented here demonstrated that the S-layer protein EA1 can self-assemble into 2D crystalline arrays in vitro, similar to the natural structure of S-layer in *B. anthracis*. Based on this observation, we developed a chimeric S-layer formed following the self-assembly of the fusion protein EA1$_{30}$–MPH. The nanosized chimeric S-layer significantly improved the stability of MPH activity. We used this S-layer for detecting anthrax-specific antibodies in the serum samples of mice. Because of the high densities of capturing molecules and signal molecules, the nanostructure rapidly captured anthrax-specific antibodies from serum samples, with a detection limit of 0.1 ng mL^{-1} by visual observations with a detection sensitivity 200–300 times higher than that for monomeric recombinant protein EA1$_{30}$–MPH. Therefore, the EA1-based nanomaterial constructed in this study might be of use as a potential and efficient tool for both enhancement of enzymatic stability and early serological diagnosis of anthrax disease. In conclusion, our study further supports the notion that bionanomaterials can be endowed with broad applications by coupling the intrinsic biological functions of biomolecules with their nanostructures.

4. Experimental Section

Plasmid, Strains, and Reagents: *E. coli* strain DH5α was used for cloning and *E. coli* M15 was used for protein expression. Plasmid pQE30 (Qiagen, Germany) was used to insert genes and transformed into either *E. coli* DH5α for cloning or *E. coli* M15 for protein expression. Triton X-100, 1-ethyl-3-[3-dimethylaminopropyl] carbodiimide (EDC), *N*-hydroxysulfosuccinimide (sulfo-NHS), 2-(*N*-morpholino) ethanesulfonic acid (MES), and bovine serum albumin (BSA) were obtained from Sigma (USA). BCA Protein Assay Kit was purchased from Thermo (USA). Restriction enzymes, DNA polymerase, and T4 ligase for plasmid construction were purchased from Takara (TaKaRa, Dalian, China). Parathion methyl was obtained from Amresco (USA). Goat anti-mouse IgG was purchased from Boster (BA1038, Wuhan, China). Carboxylated superparamagnetic iron oxide particles of 300 nm diameter were purchased from Ademtech (Pessac, France). All other reagents used were of analytical grade.

Construction of Recombinant Plasmids pQE$_{30}$–EA1$_{30}$–MPH: Because of limited restriction sites in plasmids, we first constructed pQE30–MPH, and then inserted *eag* (encoding EA1 protein) gene at the N-terminus of MPH. To construct pQE30–MPH, the gene coding MPH was cloned from pET5a-MPHs using the primer sequences: 5′-ATATCTGCAGGCCGCACCGCAGGTG-3′ and 5′-GTGAAGCTTTTACTTGGGGTTGACGAC-3′. The conditions for PCR were as follows: 94 °C for 5 min; 94 °C for 30 s, 60 °C for 30 s, and 72 °C for 1 min for 35 cycles; and lastly 72 °C for 10 min. The PCR products were inserted into plasmid pQE30 after digestion with *Pst* I and *Hind* III, and the plasmid for recombinant protein expression was transformed into *E. coli* DH5α. The DNA sequence encoding the truncated form of EA1 missing 29 amino acids at its N-terminus was amplified by PCR from a previously reported construct[18] (extension step of 160 s for 35 cycles) with primers as below: 5′-TGTAGGATCCGCAGGTAAATCATTC-3′ and 5′-GCCGAGCTCTAGATTTGGGTTATTA-3′. The PCR products were digested with *Bam*HI and *Sac*I, and then inserted into plasmid named pQE30–MPH. Lastly, the recombinant plasmids pQE30–EA1$_{30}$–MPH were transformed into *E. coli* DH5α and *E. coli* M15 for further study.

Proteins Purification and Characterization: *E. coli* M15/pQE30–EA1$_{30}$–MPH, *E. coli* M15/pQE30–EA1$_{30}$ and *E. coli* M15/pQE30–MPH were grown by shaking at 180 rpm at 37 °C in Luria-Bertani medium (LB broth: 10 g L^{-1} peptone, 5 g L^{-1} yeast extract, 10 g L^{-1} NaCl, pH 7.0) supplemented with ampicillin (100 μg mL^{-1}) and kanamycin (50 μg mL^{-1}) to an $OD_{600\ nm}$ of 0.6. Cells were then induced with 1×10^{-3} M isopropyl β-D-1-thiogalactopyranoside (IPTG) for over 5 h at 28 °C. The cells were harvested by centrifugation at 6000 rpm at 4 °C for 10 min. The cells were resuspended in buffer (20×10^{-3} M tris–HCl, 0.5 M NaCl, 10×10^{-3} M imidazole, pH 7.9) containing 2 M guanidine hydrochloride. After 30 min of ultrasonication, the cells were centrifugated at 10 000 rpm at 4 °C for 30 min. The recombinant proteins in the supernatant were purified using His Trap HP column (Novagen, USA), by stepwise application of binding buffer (20×10^{-3} M tris–HCl, 0.5 M NaCl, 10×10^{-3} M imidazole, 2 M guanidine hydrochloride, pH 7.9), washing buffer (20×10^{-3} M tris–HCl, 0.5 M NaCl, 40×10^{-3} M imidazole, 2 M guanidine hydrochloride, pH 7.9) and elution buffer (20×10^{-3} M tris–HCl, 0.5 M NaCl, 250×10^{-3} M imidazole, 2 M guanidine hydrochloride, pH 7.9). The purified proteins were dialyzed overnight at 4 °C against a buffer containing 50×10^{-3} M tris–HCl, 50×10^{-3} M NaCl pH 7.9, followed by 10% SDS–PAGE analysis. The concentrations of purified proteins were determined by BCA Protein Assay Kit (Thermo Fisher Scientific, America) using bovine serum albumin as a standard.

Self-Assembly of EA1$_{30}$ and EA1$_{30}$–MPH In Vitro and Transmission Electron Microscopy Analysis: To investigate whether EA1$_{30}$ and EA1$_{30}$–MPH can be self-assembled in vitro or not, the purified proteins were diluted into 30–100 μg mL^{-1} of assembly buffer (10×10^{-3} M $CaCl_2$, 0.5×10^{-3} M tris–HCl, pH 9.0) and were incubated at 25 °C or 4 °C for 5–12 h. The self-assembly samples were then analyzed by electron microscopy. A droplet of self-assembly sample containing 30–50 μg mL^{-1} protein was placed onto a carbon-coated copper TEM grid for 5 min, and excess solution was removed with filter paper. The sample on TEM grids was stained with 2% phosphotungstic acid for 3 min, and the excess solution was removed with filter paper. The grids were examined with a FEI Tecnai G2 20 TWIN electron microscope operating at 200 kV after they were thoroughly air-dried.

Figure 1a,f show the S-layer sheets obtained from self-assembly of EA1$_{30}$ and EA1$_{30}$–MPH, respectively. The enlarged TEM images of selected S-layer sheets were served as raw data (Figure 1b,g) to subject to Fourier transform processing. The raw data were transformed to Fourier space (Figure 1c,h) and then the filter FFT-maps (Figure 1d,i) (Here, FFT denotes fast Fourier Transform). The FFT maps were inverted back to the real maps (Figure 1e,j) by using DigitalMicrograph (Gatan Company). The differences between EA1$_{30}$ and EA1$_{30}$–MPH in the distribution of diffraction spots in the Fourier maps clearly illustrate their different regular structures.

Determination of Methyl Parathion Hydrolase Activity: Purified recombinant proteins EA1$_{30}$–MPH/MPH were dialyzed in assembly buffer (10×10^{-3} M $CaCl_2$, 0.5×10^{-3} M tris–HCl, pH 9.0) and control buffer (0.5×10^{-3} M tris–HCl, pH 7.0) for 24 h. Samples were stored at 4 °C and 37 °C at a concentration of $0.2–1 \times 10^{-6}$ M, and their MPH activity measured at regular intervals. For this procedure, 0.125×10^{-3} M parathion methyl was dissolved in 20×10^{-3} M phosphate buffer (pH 7.0) and then used as the reaction substrate. In each test, 5 μL protein samples were incubated with 200 μL reaction buffer in 96-well plates (Jet Biofil, China) for 5–15 min at room temperature to produce yellow nitrophenol, which has a specific absorption wavelength of 405 nm. Then, the activity of MPH was determined by detecting the optical density at 405 nm ($OD_{405\ nm}$) using a BioTek enzyme standard instrument (Synergy H1, BioTek, USA).

Conjugation of Goat Anti-Mouse IgG to Magnetic Particles: The goat anti-mouse IgG (Boster BA1038, Wuhan, China) was conjugated to magnetic iron oxide particles (Ademtech, Pessac, France) by chemical cross-linking. In brief, 30 mg mL^{-1} carboxylated magnetic particles of 50 μL were incubated with 1-ethyl-3-[3-dimethylaminopropyl] carbodiimide (EDC) and *N*-hydroxysulfosuccinimide in MES-buffered saline (pH 4.7) at room temperature for 2 h to form an amine-reactive sulfo-NHS ester. The above solution was then added 30 μL goat anti-mouse IgG of 10 mg mL^{-1} was added to the above solution for 2 h in 37 °C to produce amide bonds between the particles and the IgG. The residual active coupling sites on the particles were blocked with 5% BSA at 37 °C for 2 h. Finally, the conjugates were washed three times and were stored in 0.01 MPBS at 4 °C until further analysis.

Detection of Anthrax-Specific Antibodies by Self-Assembled EA1$_{30}$–MPH: Six-week-old BALB/c mice were injected subcutaneously with 10^5 vegetative cells of *B. anthracis* A16 for three times at 2 week intervals before boosting by injection of a double dose. The antibodies in these mouse sera were purified by caprylic acid–ammonium sulfate precipitation of ascites, and were then quantified by BCA Protein Assay Kit (Thermo Fisher Scientific, USA). Both antibodies and serum from mouse were used as samples for detection. First, a series of concentrations of antibodies as well as serum both diluted in PBS plus 1% BSA was incubated with the conjugates of goat anti-mouse IgG and magnetic particles at 37 °C for 20 min. After three washes with PBS containing 0.1% Tween 20 (PBST) and magnetic separations, the precipitates were incubated with assembled and unassembled EA1$_{30}$–MPH (30–50 μg mL^{-1}) for 20 min at 37 °C. After the reaction was completed, the complexes were washed three times with sodium tetraborate solution (pH 9.5) to eliminate nonspecifically bound material. Finally, the absorbance of all supernatants was measured at 405 nm using a Biotek enzyme standard instrument (Synergy H1, BioTek, USA) by

incubation with 0.25×10^{-3} M parathion methyl of 100 µL at 37 °C and magnetic separation.

Supporting Information

Supporting Information is available from the Wiley Online Library or from the author.

Acknowledgements

X.Y.W. and D.B.W. contributed equally to this work. This work was financially supported by Natural Science Foundation of China (No. 31000454) and the National High Technology Research and Development Program ("863"Program) of China (Nos. 2011AA02A114, 2012AA022206, Dian-Bing Wang). X.-E.Z. was supported by the Chinese Academy of Sciences. The authors are thankful to Dr. Bo Tian and Dr. Ding Gao for technical assistance.

[1] a) W. Reisner, J. N. Pedersen, R. H. Austin, *Rep. Prog. Phys.* **2012**, *75*, 106601; b) A. Lakshmanan, S. Zhang, C. A. Hauser, *Trends Biotechnol.* **2012**, *30*, 155; c) M. Comellas-Aragones, H. Engelkamp, V. I. Claessen, N. A. Sommerdijk, A. E. Rowan, P. C. Christianen, J. C. Maan, B. J. Verduin, J. J. Cornelissen, R. J. Nolte, *Nat. Nanotechnol.* **2007**, *2*, 635; d) E. G. Bellomo, M. D. Wyrsta, L. Pakstis, D. J. Pochan, T. J. Deming, *Nat. Mater.* **2004**, *3*, 244; e) S. Zhang, *Nat. Nanotechnol.* **2003**, *21*, 1171.

[2] M. Sara, U. B. Sleytr, *J. Bacteriol.* **2000**, *182*, 859.

[3] U. B. Sleytr, M. Sara, *Trends Biotechnol.* **1997**, *15*, 20.

[4] a) J. L. Toca-Herrera, R. Krastev, V. Bosio, S. Kupcu, D. Pum, A. Fery, M. Sara, U. B. Sleytr, *Small* **2005**, *1*, 339; b) M. H. Ucisik, S. Kupcu, M. Debreczeny, B. Schuster, U. B. Sleytr, *Small* **2013**, *9*, 2895; c) L. R. Comolli, C. E. Siegerist, S. H. Shin, C. Bertozzi, W. Regan, A. Zettl, J. De Yoreo, *Angew. Chem. Int. Ed.* **2013**, *52*, 4829.

[5] U. B. Sleytr, P. Messner, D. Pum, M. Sara, *Angew. Chem. Int. Ed.* **1999**, *38*, 1034.

[6] a) C. Vericat, M. E. Vela, G. A. Andreasen, R. C. Salvarezza, F. Borgatti, R. Felici, T. L. Lee, F. Renner, J. Zegenhagen, J. A. Martin-Gago, *Phys. Rev. Lett.* **2003**, *90*, 075506; b) S. R. Scheicher, B. Kainz, S. Kostler, N. Reitinger, N. Steiner, H. Ditlbacher, A. Leitner, D. Pum, U. B. Sleytr, V. Ribitsch, *Biosens. Bioelectron.* **2013**, *40*, 32; c) M. M. Picher, S. Kupcu, C. J. Huang, J. Dostalek, D. Pum, U. B. Sleytr, P. Ertl, *Lab Chip.* **2013**, *13*, 1780; d) M. Rothbauer, S. Kupcu, D. Sticker, U. B. Sleytr, P. Ertl, *ACS Nano* **2013**, *7*, 8020.

[7] a) B. Schuster, D. Pum, M. Sára, O. Braha, H. Bayley, U. B. Sleytr, *Langmuir* **2001**, *17*, 499; b) W. Shenton, D. Pum, U. B. Sleytr, S. Mann, *Nature* **1997**, *389*, 585; c) J. Liu, Y. Mao, E. Lan, D. R. Banatao, G. J. Forse, J. Lu, H. O. Blom, T. O. Yeates, B. Dunn, J. P. Chang, *J. Am. Chem. Soc.* **2008**, *130*, 16908.

[8] a) D. Moll, C. Huber, B. Schlegel, D. Pum, U. B. Sleytr, M. Sara, *Proc. Natl. Acad. Sci. USA* **2002**, *99*, 14646; b) M. Duval, C. J. Lewis, J. F. Nomellini, M. S. Horwitz, J. Smit, L. A. Cavacini, *Antimicrob. Agents Chemother.* **2011**, *55*, 5547; c) C. Schaffer, R. Novotny, S. Kupcu, S. Zayni, A. Scheberl, J. Friedmann, U. B. Sleytr, P. Messner, *Small* **2007**, *3*, 1549.

[9] a) C. Horejs, H. Gollner, D. Pum, U. B. Sleytr, H. Peterlik, A. Jungbauer, R. Tscheliessnig, *ACS Nano* **2011**, *5*, 2288; b) E. Baranova, R. Fronzes, A. Garcia-Pino, N. Van Gerven, D. Papapostolou, G. Pehau-Arnaudet, E. Pardon, J. Steyaert, S. Howorka, H. Remaut, *Nature* **2012**, *487*, 119; c) F. Baneyx, J. F. Matthaei, *Curr. Opin. Biotechnol.* **2014**, *28*, 39.

[10] S. Mesnage, E. Tosi-Couture, M. Mock, P. Gounon, A. Fouet, *Mol. Microbiol.* **1997**, *23*, 1147.

[11] S. S. Makam, J. J. Kingston, M. S. Harischandra, H. V. Batra, *Mol. Immunol.* **2014**, *59*, 91.

[12] E. Shlyakhov, Y. Shoenfeld, B. Gilburd, E. Rubinstein, *Clin. Microbiol. Infect.* **2004**, *10*, 421.

[13] Y. L. Chen, X. E. Zhang, H. Liu, Y. S. Wang, X. M. Xia, *Acta Microbiol. Sin.* **2002**, *42*, 490.

[14] L. L. Liu, Y. F. Zhou, Z. P. Zhang, H. Liu, X. E. Zhang, *Microbiology* **2004**, *31*, 77.

[15] W. Yang, Y. F. Zhou, H. P. Dai, L. J. Bi, Z. P. Zhang, X. H. Zhang, Y. Leng, X. E. Zhang, *Anal. Bioanal. Chem.* **2008**, *390*, 2133.

[16] C. P. Quinn, V. A. Semenova, C. M. Elie, S. Romero-Steiner, C. Greene, H. Li, K. Stamey, E. Steward-Clark, D. S. Schmidt, E. Mothershed, J. Pruckler, S. Schwartz, R. F. Benson, L. O. Helsel, P. F. Holder, S. E. Johnson, M. Kellum, T. Messmer, W. L. Thacker, L. Besser, B. D. Plikaytis, T. H. Taylor Jr., A. E. Freeman, K. J. Wallace, P. Dull, J. Sejvar, E. Bruce, R. Moreno, A. Schuchat, J. R. Lingappa, S. K. Martin, J. Walls, M. Bronsdon, G. M. Carlone, M. Bajani-Ari, D. A. Ashford, D. S. Stephens, B. A. Perkins, *Emerging Infect. Dis.* **2002**, *8*, 1103.

[17] E. Couture-Tosi, H. Delacroix, T. Mignot, S. Mesnage, M. Chami, A. Fouet, G. Mosser, *J. Bacteriol.* **2002**, *184*, 6448.

[18] D. B. Wang, R. Yang, Z. P. Zhang, L. J. Bi, X. Y. You, H. P. Wei, Y. F. Zhou, Z. Yu, X. E. Zhang, *PloS One* **2009**, *4*, e7810.

Received: May 18, 2015
Revised: July 28, 2015
Published online: September 30, 2015